Since January 2020 Elsevier has created a COVID-19 resource centre with free information in English and Mandarin on the novel coronavirus COVID-19. The COVID-19 resource centre is hosted on Elsevier Connect, the company's public news and information website.

Nano Today 40 (2021) 101243

Contents lists available at ScienceDirect

Nano Today

journal homepage: www.elsevier.com/locate/nanotoday

TiO_2 supported single Ag atoms nanozyme for elimination of SARS-CoV2

Daji Wang[a,1], Bin Zhang[a,1], Hui Ding[a,1], Dan Liu[c], Jianquan Xiang[b], Xuejiao J. Gao[e], Xuehui Chen[c], Zhongjun Li[a], Lei Yang[a], Hongxia Duan[c], Jiyan Zheng[c], Zheng Liu[c], Bing Jiang[c], Yang Liu[a], Ni Xie[a], Han Zhang[d], Xiyun Yan[a,c,f,*], Kelong Fan[c,f,**], Guohui Nie[a,***]

[a] Shenzhen Key Laboratory of nanozymes and Translational Cancer Research, Department of Otolaryngology, and Institute of Translational Medicine, Shenzhen Second People's Hospital/the First Affiliated Hospital of Shenzhen University Health Science Center, Shenzhen 518035, China
[b] School of Basic Medical Sciences, Southwest Medical University, Sichuan 646000, China
[c] CAS Engineering Laboratory for Nanozyme, Key Laboratory of Protein and Peptide Pharmaceuticals, Institute of Biophysics, Chinese Academy of Sciences, Beijing 100101, China
[d] SZU-NUS Collaborative Innovation Center for Optoelectronic Science & Technology, International Collaborative Laboratory of 2D Materials for Optoelectronics Science and Technology of Ministry of Education College of Physics and Optoelectronic Engineering Shenzhen University, Shenzhen 518060, China
[e] College of Chemistry and Chemical Engineering, Jiangxi Normal University, Nanchang 330022, China
[f] Nanozyme Medical Center, School of Basic Medical Sciences, Zhengzhou University, Zhengzhou 450001, China

ARTICLE INFO

Article history:
Received 14 October 2020
Received in revised form 8 June 2021
Accepted 1 July 2021
Available online 7 July 2021

Keywords:
Single-atom nanozyme
Neutralization
Peroxidase-like activity
Reactive oxygen species
Anti-SARS-CoV2

ABSTRACT

The outbreak of SARS-coronavirus 2 (SARS-CoV2) has become a global health emergency. Although enormous efforts have been made, there is still no effective treatment against the new virus. Herein, a TiO_2 supported single-atom nanozyme containing atomically dispersed Ag atoms (Ag-TiO_2 SAN) is designed to serve as a highly efficient antiviral nanomaterial. Compared with traditional nano-TiO_2 and Ag, Ag-TiO_2 SAN exhibits higher adsorption (99.65%) of SARS-CoV2 pseudovirus. This adsorption ability is due to the interaction between SAN and receptor binding domain (RBD) of spike 1 protein of SARS-CoV2. Theoretical calculation and experimental evidences indicate that the Ag atoms of SAN strongly bind to cysteine and asparagine, which are the most abundant amino acids on the surface of spike 1 RBD. After binding to the virus, the SAN/virus complex is typically phagocytosed by macrophages and colocalized with lysosomes. Interestingly, Ag-TiO_2 SAN possesses high peroxidase-like activity responsible for reactive oxygen species production under acid conditions. The highly acidic microenvironment of lysosomes could favor oxygen reduction reaction process to eliminate the virus. With hACE2 transgenic mice, Ag-TiO_2 SAN showed efficient anti-SARS-CoV2 pseudovirus activity. In conclusion, Ag-TiO_2 SAN is a promising nanomaterial to achieve effective antiviral effects for SARS-CoV2.

Introduction

In December 2019, a new infectious respiratory disease emerged, causing fever, severe respiratory illness, and pneumonia [1,2]. Various studies showed that it is caused by a new severe acute respiratory syndrome β-coronavirus (SARS-CoV2), and hence the disease was named coronavirus disease 2019 (COVID-19) [3]. COVID-19 is the third large-scale pandemic caused by coronavirus in the last two decades after SARS and Middle East Respiratory Syndrome (MERS) [4,5]. The number of laboratory-confirmed COVID-19 cases is already more than 90 times higher than the total number of confirmed cases of SARS and MERS [6]. Thus, SARS-CoV2 is posing a serious threat to global public health. There is an urgent need for specific anticoronavirus therapeutics and prophylactics for treatment and prevention.

Nanomaterials possess considerable potential for antimicrobial application [7–10]. Recently, Bonam et al. summarized the rationale applications of nanomedicine against Coronaviruses [11]. Especially for SARS-CoV2, various nanomaterials have shown promising

* Corresponding author at: Shenzhen Key Laboratory of nanozymes and Translational Cancer Research, Department of Otolaryngology, and Institute of Translational Medicine, Shenzhen Second People's Hospital/the First Affiliated Hospital of Shenzhen University Health Science Center, Shenzhen 518035, China.
** Corresponding author at: CAS Engineering Laboratory for Nanozyme, Key Laboratory of Protein and Peptide Pharmaceuticals, Institute of Biophysics, Chinese Academy of Sciences, Beijing 100101, China.
*** Corresponding author.
E-mail addresses: yanxy@ibp.ac.cn (X. Yan), fankelong@ibp.ac.cn (K. Fan), nieguohui@email.szu.edu.cn (G. Nie).
[1] These authors contributed equally to this work.

https://doi.org/10.1016/j.nantod.2021.101243
1748-0132/

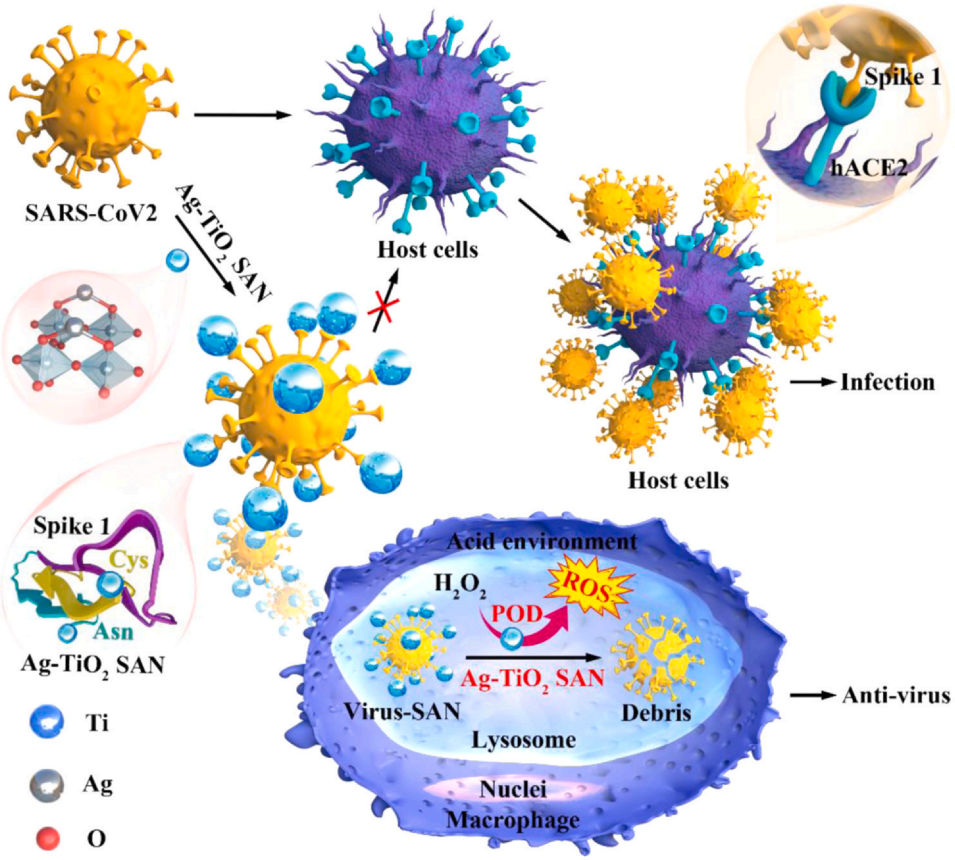

Scheme 1. Schematic of Ag-TiO_2 SAN with anti-SARS-CoV2 activity.

antiviral activity [12,13]. Compared to traditional materials, nanomaterials are superior because of their small size, large specific surface area, high adsorption and catalytic capacity [14]. Many nanomaterials have been reported to have a binding preference for amino acids or peptides. For instance, peptides have been reported to interact with the surface of gold nanoparticles (NPs) through cysteine residues or attach to the surface by a combination of several non-cysteine amino acids (*i.e.*, tyrosine, serine, lysine, aspartic acid) *via* multidentate binding [15]. Sarikaya et al. used a set of experimentally determined quartz binding peptides with different affinities to quartz (10 strong, 14 moderate, and 15 weak peptide binders to quartz) [16]. Of note, Yacaman et al. designed 1–10 nm Ag NPs, which specifically interact with sulfur-bearing residues on the gp120 glycoprotein of human immunodeficiency virus 1 (HIV-1) [17], indicating that nanomaterials have advantages in antimicrobial application. Importantly, nanomaterials harboring intrinsic enzyme-like activity have been identified [18–21]. These characteristics of nanomaterials prompted us to design a novel material that specifically absorbs to SARS-CoV2 and subsequently eliminate the virus. Among various inorganic materials, Ag and TiO_2 NPs are considered effective antimicrobial agents. Nano-Ag is one of the promising nanomaterial microbicides due to its effectiveness (even at small doses) and minimal toxicity and side effects [22]. Nano-Ag shows high adsorption to microbes and subsequently produces Ag^+ and reactive oxygen species (ROS), which are responsible for microbial shell breakdown [23–25]. Nano-TiO_2 is another biocompatible nanomaterial that can be excited by near-ultraviolet rays and possesses photochemical sterilization and self-cleaning capabilities [26,27]. The photochemical sterilization effects of nano-TiO_2 have been intensively investigated on a wide spectrum of organisms, including virus, bacteria and tumor cells [28–30]. Although significant progress has been made in nanomaterial research, improving the biocatalytic sites of nanomaterials poses a major challenge due to the inhomogeneity of traditional nanomaterials.

Single-atom nanozymes (SANs), which are defined as mimic enzyme containing only isolated single metal atoms on various substrates with atomically dispersed metal centers, maximize the atomic utilization efficiency and density of active sites [31]. In addition, the homogeneous structure of SANs facilitates the accurate discernment and characterization of active sites, thus providing deep insight into the construction of desirable SANs for high-performance catalysis at the atomic level in the biological milieu [32,33]. Consequently, the intrinsic physiochemical and catalytic features of SANs make them intriguing candidates for the design of highly efficient biocatalysts and for pioneering new paradigms in promoting beneficial catalytic reactions for desirable biomedical applications. In addition, such atomically dispersed metal catalysts have also found applications in the chemical engineering industry due to their superior catalytic performance compared with corresponding metal nanocatalysts, especially in value-added chemical production, energy transformation and environmental protection [34]. Among these applications, quite a few metal single-atom catalysts have demonstrated intriguing potential for activating O_2 molecules, which offers the possibility to catalyze the formation of singlet O_2, thus being promising for biomedicines. Our group is devoted to exploring the strategies for synthesizing single-atom catalysts with precise and uniform gram-scale structures, which is key for future applications [35,36]. Many studies have shown that SANs exhibit very strong antibacterial and antiviral effects [37–39], which led us to consider SANs as a nanomaterial against SARS-CoV2.

Here, we successfully designed Ag-TiO_2 SAN, and demonstrated that the SAN exhibits excellent anti-SARS-CoV2 activity. This novel SAN exhibits enhanced *in vitro* absorption with a rate of up to 99.65% for SARS-CoV2 pseudovirus, which highly expresses spike protein of

SARS-CoV2 on HIV-1 surface. Theoretical calculations and experimental evidences indicate that Ag atoms of SAN strongly bind to cysteine and asparagine, which are the most abundant amino acids on the surface of spike 1 protein. *In vivo*, the SAN efficiently promotes virus phagocytosis by macrophages. The intrinsic peroxidase-like activity of Ag-TiO_2 SAN exerts promising antiviral effects in lysosomes. With viral elimination models, we found that Ag-TiO_2 SAN significantly eliminates pseudovirus, which could protect host cells from infection (Scheme 1). In addition, gram-scale SANs can be produced *via* an energy- and cost-efficient approach. This study provides new insight for employing anti-SARS-CoV2 nanomaterials.

Results and discussion

Characterization of Ag-TiO_2 SAN

One gram of Ag-TiO_2 SAN was prepared *via* a wet chemistry method in one batch, with the loading of Ag determined as 1.0 wt% *via* inductively coupled plasma optical emission spectrometry (ICP-OES). Anatase TiO_2 with a size of 5–10 nm was selected as the support, due to the uniform crystalline structure and surface arrangement, which is beneficial for precisely conducting site-specific studies and mechanistic investigations. TiO_2 has a small size advantage over larger ones, resulting in easier passive targeting and larger surface area, which could load more metals or drug molecules. The geometric structure of Ag-TiO_2 SAN was characterized (Fig. 1a). Scanning electron microscopy (SEM) and dynamic light scattering (DLS) experiments were first employed for checking whether the decoration of Ag led to aggregation of TiO_2; the results showed that the SAN is uniformly distributed and the size of SAN is 10–15 nm (Fig. 1b-c). As shown in Fig. 1d-e, Ag was atomically dispersed on the TiO_2 support in Ag-TiO_2 SAN, with Ag, Ti, and O elements well distributed across the space. In comparison, when observing Ag NPs, particles with a size of 3–5 nm were detected (Fig. 1f-g). Further, the Ag-TiO_2 interaction was investigated by Raman and solid ultraviolet–visible (UV–vis) spectroscopy (Fig. 1h). The peak around 450 nm was ascribed to Ag species whose size is larger than 3 nm, further confirming the existence of Ag NPs. Fig. 1i manifests that the characteristic peak of TiO_2 was maintained before and after Ag doping, but the Eg value increased, which is more prominent in SAN. Furthermore, the UV–vis spectra indicate that the bandgaps of TiO_2 decreased obviously in both Ag/TiO_2 (Ag-TiO_2 SAN) and Ag NPs/TiO_2, with Eg values of 2.99 eV and 2.84 eV, respectively. These observations serve as solid and unambiguous evidence for the strong metal-support interaction in these two materials, and different electronic structures offer supported Ag materials good potential for outperforming TiO_2 in catalytic reactions.

Ag-TiO_2 SAN exhibits high adsorption ability for SARS-CoV2 pseudovirus

In order to evaluate anti-virus effects of Ag-TiO_2 SAN, we firstly introduced the pseudovirus, which expresses spike protein of SARS-CoV2 on HIV-1 surface and carries luciferase reporter protein internally. We overexpressed human angiotensin converting enzyme 2 (hACE2) in 293T cells (hACE2^{OE}-293T). The overexpression of hACE2 was confirmed by the mRNA and protein levels (Figure S1a-c). In our

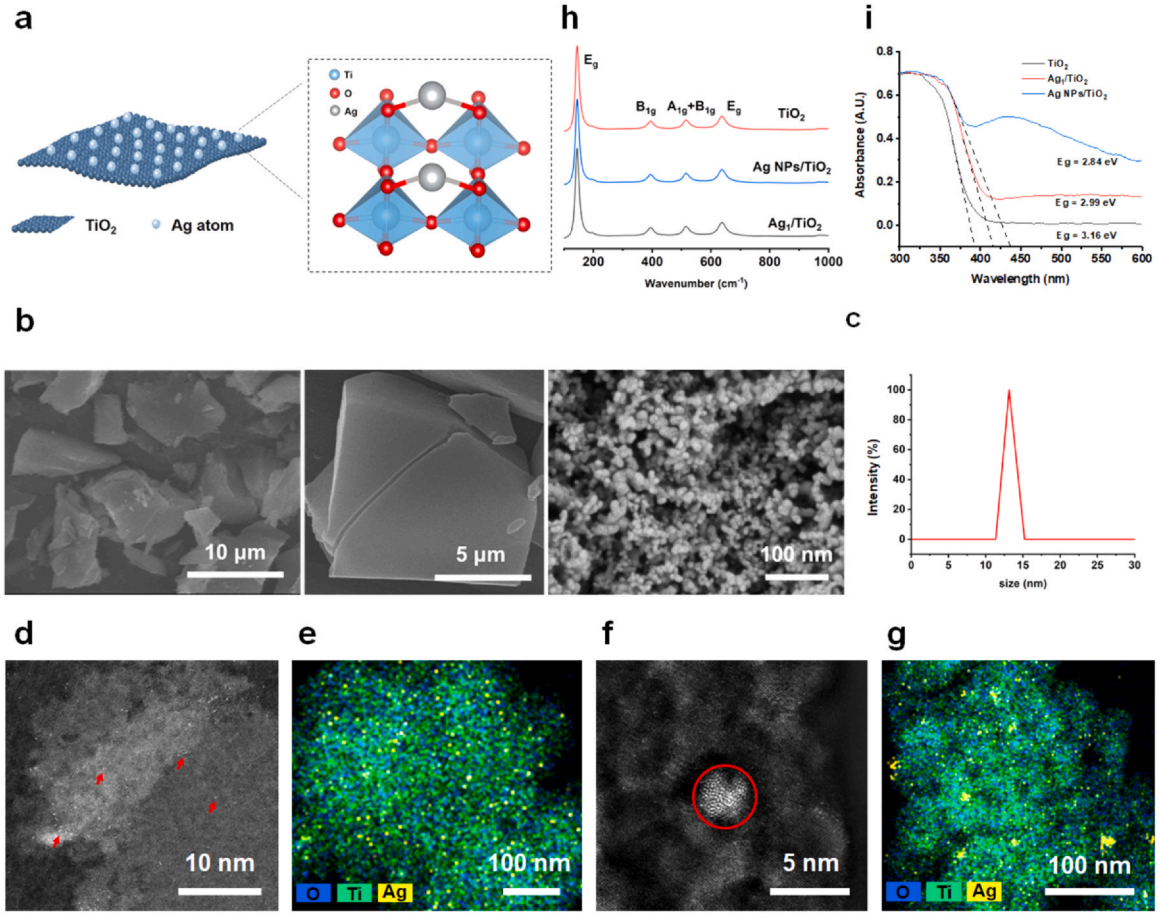

Fig. 1. Characterization of Ag-TiO_2 SAN. (a) Schematic of Ag-TiO_2 SAN. (b) SEM images of Ag-TiO_2 SAN. (c) DLS analysis of Ag-TiO_2 SAN. (d and f) HAADF-STEM images of (d) Ag-TiO_2 SAN and (f) Ag NPs/TiO_2 and corresponding EDX mapping (e) for Ag-TiO_2 SAN and (g) for Ag NPs/TiO_2. (h and i) Raman and UV–vis spectra of Ag-TiO_2 SAN, TiO_2 and Ag NPs/TiO_2.

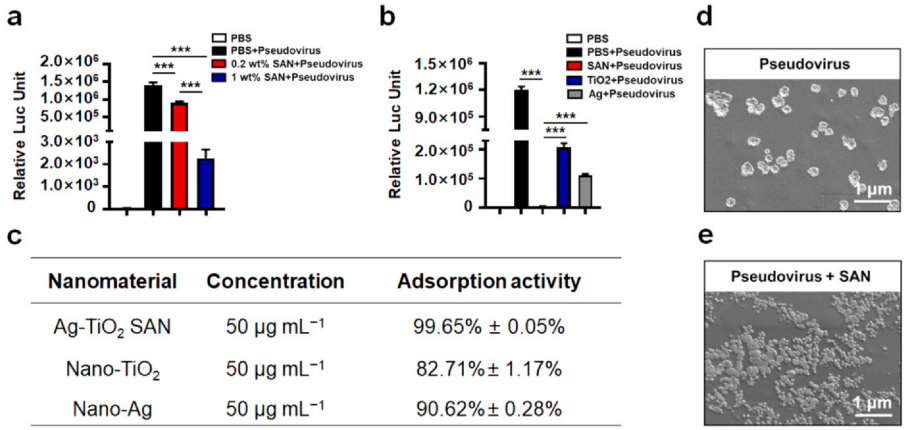

c

Nanomaterial	Concentration	Adsorption activity
Ag-TiO_2 SAN	50 μg mL^{-1}	99.65% ± 0.05%
Nano-TiO_2	50 μg mL^{-1}	82.71%± 1.17%
Nano-Ag	50 μg mL^{-1}	90.62%± 0.28%

Fig. 2. The adsorption by Ag-TiO_2 SAN of SARS-CoV2 pseudovirus. (a) The adsorption of SARS-CoV2 pseudovirus by 0.2 wt% and 1 wt% Ag loaded SANs. The PBS as negative control, PBS + SARS-CoV2 as positive control. (b) $10^{4.5}$ $TCID_{50}$ pseudovirus was treated with Ag-TiO_2 SAN, nano-Ag, and nano-TiO_2 for 1 h at room temperature. The supernatants were used to infect $hACE2^{OE}$-293T cells. Luciferase activity was detected after 72 h. The PBS as negative control, PBS + SARS-CoV2 as positive control. (c) Statistics of adsorption activities of Ag-TiO_2 SAN, nano-Ag and nano-TiO_2 for SARS-CoV2 pseudovirus. (d-e) SEM images of SARS-CoV2 pseudovirus and SAN/pseudovirus complexes.

in vitro viral infection assay, the ability of pseudovirus to infect $hACE2^{OE}$-293T was obviously higher than wild type 293T cells ($hACE2^{WT}$-293T, Figure S2).

To determine the proper concentrations of Ag-TiO_2 SAN, nano-TiO_2 and nano-Ag for the experiments, we evaluated the viability of cells treated by these nanomaterials in the concentration range from 0 to 300 μg mL^{-1} for 72 h. The results showed that cell viability was more than 95% when treated with 1 wt% Ag loaded SAN, nano-TiO_2, or nano-Ag at a concentration of 50 μg mL^{-1} (Figure S3a). Cell integrity was not affected at this concentration (Figure S3b). In addition, we evaluated the dissolution of Ag during the storage of 1 wt% Ag loaded SAN. ICP-MS result showed that the silver content in Ag NPs solution (10 mg mL^{-1}) was 11.4 ± 1.25 ng mL^{-1}, while the silver level (1.0 ± 0.46 ng mL^{-1}) in Ag-TiO_2 SAN solution (10 mg mL^{-1}) was much lower due to Ag being only 1 wt% of the SAN (Figure S4), indicating the limited toxic of Ag-TiO_2 SAN.

Next, we analyzed the adsorption ability of 0.2 wt% and 1 wt% Ag atom loaded SANs for SARS-CoV2 pseudovirus. The result showed that 1 wt% Ag loaded SAN exhibits higher adsorption of pseudovirus compared with 0.2 wt% Ag loaded SAN (Fig. 2a). Thus, the high adsorption of 1 wt% Ag loaded SAN is due to surficial Ag atoms ratio. We also analyzed the adsorption ability of 1 wt% Ag loaded SAN, nano-TiO_2 and nano-Ag for pseudovirus. Surprisingly, 1 wt% Ag loaded SAN exhibits 99.65% adsorption ability for pseudovirus compared with 82.71% for nano-TiO_2 and 90.62% for nano-Ag (Fig. 2b-c). Consistently, 50 μg mL^{-1} Ag-TiO_2 SAN (1 wt% Ag) also exhibited promising adsorption ability for spike 1 protein of SARS-CoV2 (Figure S5). Thus, 1 wt% Ag loaded SAN was used for further experiments. Finally, we confirmed the direct interaction between the SAN and pseudovirus by SEM. Interestingly, we observed that the Ag-TiO_2 SAN (smaller particles) was absorbed to the pseudovirus (bigger particles) surface (Fig. 2d-e). In the skin test assay, Ag-TiO_2 SAN and nano-TiO_2 have no influence on mouse skin. However, nano-Ag severely damages the cuticle of mouse skin (Figure S6), suggesting that Ag-TiO_2 SAN has a broad application in viral adsorption, such as face mask coating and disinfectant.

Ag-TiO_2 SAN interacts with spike protein of SARS-CoV2

Spike protein is the outermost structure on SARS-CoV2, and is responsible for binding to host cells. Furthermore, 1 wt% Ag loaded SAN exhibited better adsorption of pseudovirus compared with 0.2 wt% Ag loaded SAN. Thus, we speculate that this adsorption is partially dependent on the interaction of Ag atoms and spike protein. To test this hypothesis, we incubated RBD of spike 1 protein (S1 RBD, 51 KD) with Ag-TiO_2 SAN, nano-TiO_2, nano-Ag and a mass ratio as 1:1 mixture of nano-TiO_2/Ag, and collected the supernatant for cell immunofluorescence assay. As shown in Fig. 3a-b, Ag-TiO_2 SAN exhibited higher adsorption of S1 RBD than nano-TiO_2, nano-Ag and the nano-TiO_2/Ag mixture. To confirm this result, we measured the S1 RBD levels in precipitates and supernatants of nanomaterial incubated by western blot. The results show that Ag-TiO_2 SAN binds to more S1 RBD than nano-TiO_2 and nano-Ag (Fig. 3e). The opposite results were detected in the supernatant (Fig. 3f). In addition, we performed immuno-precipitation assay to evaluate the ratio of the SANs that are bound to S1 RBD. The results show that 0.85 ± 0.12 μg SANs bound to 1 μg S1 RBD (Figure S7).

Spike protein of SARS-CoV2, unlike that of other β-B coronaviruses, harbors a special S1/S2 furin-recognizable site, indicating that its spike protein might possess some unique infectious properties. Lu et al. reported that a typical syncytium structure naturally formed by SARS-CoV2 infected cells, which is mediated by spike protein [40]. To investigate whether Ag-TiO_2 SAN interferes with spike-mediated cell-cell fusion, we transfected 293 T cells with spike protein-GFP reporter as the effector cells (Figure S8a-c) and used $hACE2^{OE}$-293T as the target cells. We first sorted GFP positive cells and incubated with Ag-TiO_2 SAN, nano-TiO_2, nano-Ag, and nano-TiO_2/Ag mixture (mass ratio as 1:1). After effector cells and target cells were cocultured at 37 °C for 2 h, the fused cells were at least twice large as normal cells. In the Ag-TiO_2 SAN treated group, spike-mediated cell-cell fusion was significantly inhibited compared with the PBS treated group, even though nano-TiO_2, nano-Ag, and nano-TiO_2/Ag treatment also inhibit cell-cell fusion to different degrees (Fig. 3c-d), indicating that the SAN serves as a blocker for virus entering into host cells. To directly demonstrate the interaction between Ag-TiO_2 SAN and S1 RBD of SARS-CoV2, we cocultured S1 RBD (2 μg) and Ag-TiO_2 SAN (50 μg mL^{-1}) at room temperature for 1 h. Energy disperse spectroscopy (EDS) analysis showed that the spike-Ag-TiO_2 SAN complex was formed (Fig. 3g), suggesting a direct interaction between Ag-TiO_2 SAN and spike protein of SARS-CoV2 takes place.

Human angiotensin converting enzyme 2 (hACE2) is considered to be one major receptor of spike protein mediating SARS-CoV2 infection to host cells [41]. However, whether the adsorption by Ag-TiO_2 SAN of SARS-CoV2 could interfere with the interaction between S1 RBD and hACE2 remains unclear. To answer this question, we

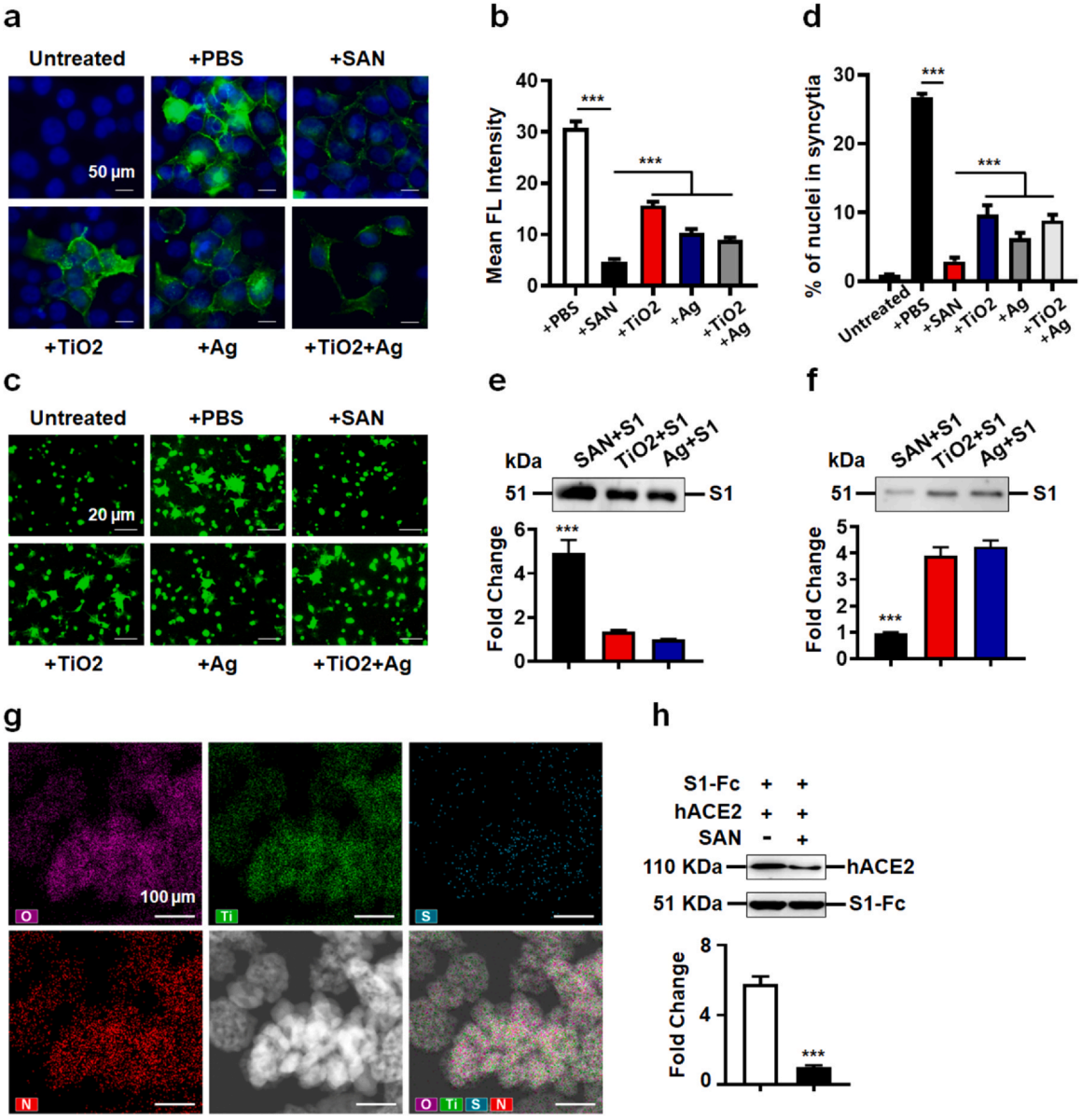

Fig. 3. Ag-TiO_2 SAN interacts with spike protein of SARS-CoV2. (a-b) Immunofluorescence images showing the absorption by nanomaterials of S1 RBD. Untreated group represents $hACE2^{OE}$-293T cells without incubation of S1 RBD. (c-d) SARS-CoV2 spike protein mediated cell-cell fusion of $hACE2^{OE}$-293T cells is blocked by Ag-TiO_2 SAN. Untreated group represents $hACE2^{OE}$-293T cells without any treatments. (e) Western blot showing the S1 RBD on Ag-TiO_2 SAN, nano-Ag and nano-TiO_2. (f) Western blot showing the S1 RBD levels remaining in the supernatant. (g) Energy dispersive spectrometry (EDS) analysis of the S1 RBD/Ag-TiO_2 SAN complex. (h) The interaction of S1 RBD and hACE2 is blocked by Ag-TiO_2 SAN.

performed pulldown assay *in vitro*. Interestingly, the ability of S1 RBD binds to hACE2 is significantly inhibited by Ag-TiO_2 SAN (Fig. 3h). Furthermore, enzyme linked immunosorbent assay (ELISA) were performed to further evaluate this inhibition. As shown in Figure S9a, the interaction of Ag-TiO_2 SAN and S1 RBD is negligibly affected by serum proteins. Importantly, compared with nano-TiO_2 and nano-Ag, the SAN exhibited the best blocking effect for binding of S1 RBD and hACE2 (Figure S9b). Together, these data demonstrate that Ag-TiO_2 SAN possesses high affinity for S1 RBD of SARS-CoV2, and this adsorption protects host cells from SARS-CoV2 infection.

Peroxidase-like activity and kinetic analysis of Ag-TiO_2 SAN

Nanomaterials can catalyze the production of high levels of reactive oxygen species (ROS), depending on intrinsic nanozyme activity, which is another approach to achieve antimicrobial effects [38,42]. Therefore, we next tested whether Ag-TiO_2 SAN possesses peroxidase-like activity, catalyzing the conversion of hydrogen peroxide (H_2O_2) into hydroxyl radicals. As shown in Fig. 4a and Figure S10a-c, Ag-TiO_2 SAN effectively catalyzed the oxidation of 3,3′,5,5′-tetramethylbenzidine (TMB) in the presence of H_2O_2 in a concentration, pH and temperature-dependent manner. The optimal pH and temperature were approximately 5.0 and 35 °C, respectively, which are similar to those of natural horseradish peroxidase (4.5 and 35 °C). In addition, the optimal pH and temperature of Ag-TiO_2 SAN are similar to those of nano-Ag, suggesting the peroxidase-like activity of Ag-TiO_2 SAN is mainly dependent on Ag atoms. Of note, 1 wt % Ag-doped Ag-TiO_2 SAN exhibited higher peroxidase-like activity than traditional nano-Ag, suggesting the efficient utilization of SAN. To analyze the catalytic activity of Ag-TiO_2 SAN, we calculated the

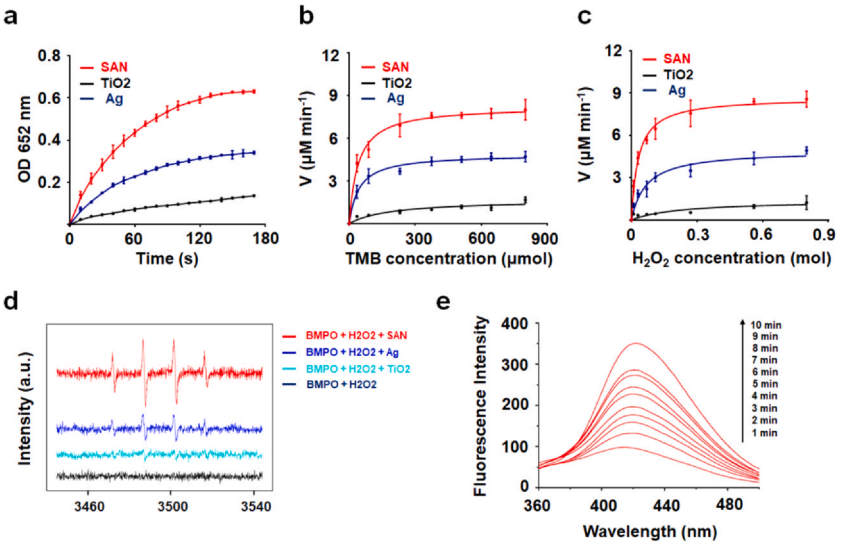

Fig. 4. Characterization of peroxidase-like kinetics of Ag-TiO_2 SAN. (a) Reaction–time curves of the colorimetric reaction of TMB catalyzed by Ag-TiO_2 SAN (red), nano-Ag (blue), and nano-TiO_2 (black). (b-c) Michaelis–Menten curves for Ag-TiO_2 SAN (red), nano-Ag (blue), and nano-TiO_2 (black). (d) Generation of hydroxyl radicals by related nanomaterials with peroxidase-like catalysis. (e) Generation of hydroxyl radicals by Ag-TiO_2 SAN, as characterized by the change in fluorescence spectra in the presence of TA.

Michaelis-Menten constant (K_M) (Fig. 4b-c). K_M, which represents the affinity of substrates to the enzyme. The K_M value was 39.9 mM for H_2O_2 and 0.032 mM for TMB (Table S1).

To the best of our knowledge, hydroxyl radicals can cause damage to viral components, inactivating the viral proteins and nucleic acids[43–45]. Therefore, it is important to determine the generation of hydroxyl radicals by Ag-TiO_2 SAN. We added H_2O_2 to the Ag-TiO_2 SAN system and measured the amounts of hydroxyl radicals by electron spin resonance (ESR) (Fig. 4d). Based on these results, we determined the ability of Ag-TiO_2 SAN to generate hydroxyl radicals. Terephthalic acid (TA) was used to indirectly detect the concentration of hydroxyl radicals. As shown in Fig. 4e, the generation of hydroxyl radicals is increased with time, even though the pH was close to neutral. These results suggest that Ag-TiO_2 SAN could steadily induce the generation of hydroxyl radicals by catalyzing the decomposition of H_2O_2.

Pharmacokinetics and biocompatibility of intravenously injected Ag-TiO_2 SAN

The pharmacokinetics of the intravenously injected sequential Ag-TiO_2 SAN were assessed to reveal its *in vivo* behavior. Initially, the time-dependent biodistribution of Ag-TiO_2 SAN in the major organs was studied. The results show that Ag-TiO_2 SAN is mainly distributed in liver, spleen, and lung tissue because of the capture by the reticuloendothelial and vascular system (Fig. 5a). In the blood-circulation experiment, a circulating half-life in the bloodstream of 3.76 h was obtained (Fig. 5b).

Toxic side effects for normal organs have been the main problem in the application of nanomaterials. Therefore, we first tested the biocompatibility of Ag-TiO_2 SAN. The results show no significant difference in mouse body weight after persistent treatment with PBS (control) and Ag-TiO_2 SAN (2–10 mg kg^{-1}) for 24 days (Fig. 5c). Furthermore, the bleeding and clotting times were not affected by 10 mg kg^{-1} Ag-TiO_2 SAN (Fig. 5d-e). To investigate whether Ag-TiO_2 SAN inflicts damage to organs, histological examination (HE) staining of various major organs (heart, liver, spleen, lung, and kidney) from mice injected with PBS and Ag-TiO_2 SAN was conducted to investigate the biological toxicity (Fig. 5f). No obvious pathological abnormality or inflammation was observed from both groups. Overall, these results firmly show the *in vivo* biocompatibility of Ag-TiO_2 SAN, potentiating its further application as antiviral agent.

Ag-TiO_2 SAN eliminates SARS-CoV2 pseudovirus in vivo

Abundant proteins in body fluids/blood such as albumin may affect the *in vivo* adsorption ability of Ag-TiO_2 SAN for virus particles. To exclude these effects, the SAN was treated with human serum/S1 RBD and PBS/S1 RBD mixture, respectively. We found that the SAN remained exhibiting high adsorption of S1 RBD in the presence of serum (Fig. 6a). Moreover, the interaction between Ag-TiO_2 SAN with S1 RBD, or pseudovirus was negligibly affected by serum proteins, even in the case of directly mixing with serum (Figure S11a-b). Furthermore, the peroxidase-like activity was negligibly affected by serum proteins (Figure S12). With antiviral assay *in vitro*, we found that the residual virus in supernatant of virus/SAN/H_2O_2 significantly decreased compared with those of only virus and virus/H_2O_2 groups. Moreover, antiviral activity of Ag-TiO_2 SAN was not affected by serum (Figure S13a). Similarly, we cocultured S1 RBD, SAN and H_2O_2, with or without serum for 1 h at room temperature. The results showed that S1 RBD was significantly degraded regardless of the presence of serum or not (Figure S13b). These results suggest that the anti-viral effect of Ag-TiO_2 SAN is negligibly affected by serum proteins.

To better understand the binding characteristics of Ag-TiO_2 SAN and S1 RBD, X-ray photoelectron spectroscopy (XPS) was conducted to compare the binding energies of N 1s and S 2p electrons. For N 1s, the peak locations of S1 RBD (Figure S14a) were unchanged after incubation with nano-TiO_2 (Figure S14b) and Ag-TiO_2 SAN (Figure S14c). Of note, XPS results of S 2p help to characterize the interaction between Ag-TiO_2 SAN and S1 RBD. Compared with the XPS of S1 RBD or S1 RBD-TiO_2 complex (Figure S14d-e), the electronic state of S changed only with the S1 RBD-SAN complex (Figure S14f). The intrinsically strong coordinating interaction between Ag and S assisted the active targeting of Ag-TiO_2 SAN toward the SARS-CoV2 pseudovirus. The interaction between Ag and S is consistent with other reports [46,47]. To further confirm the specific combination between

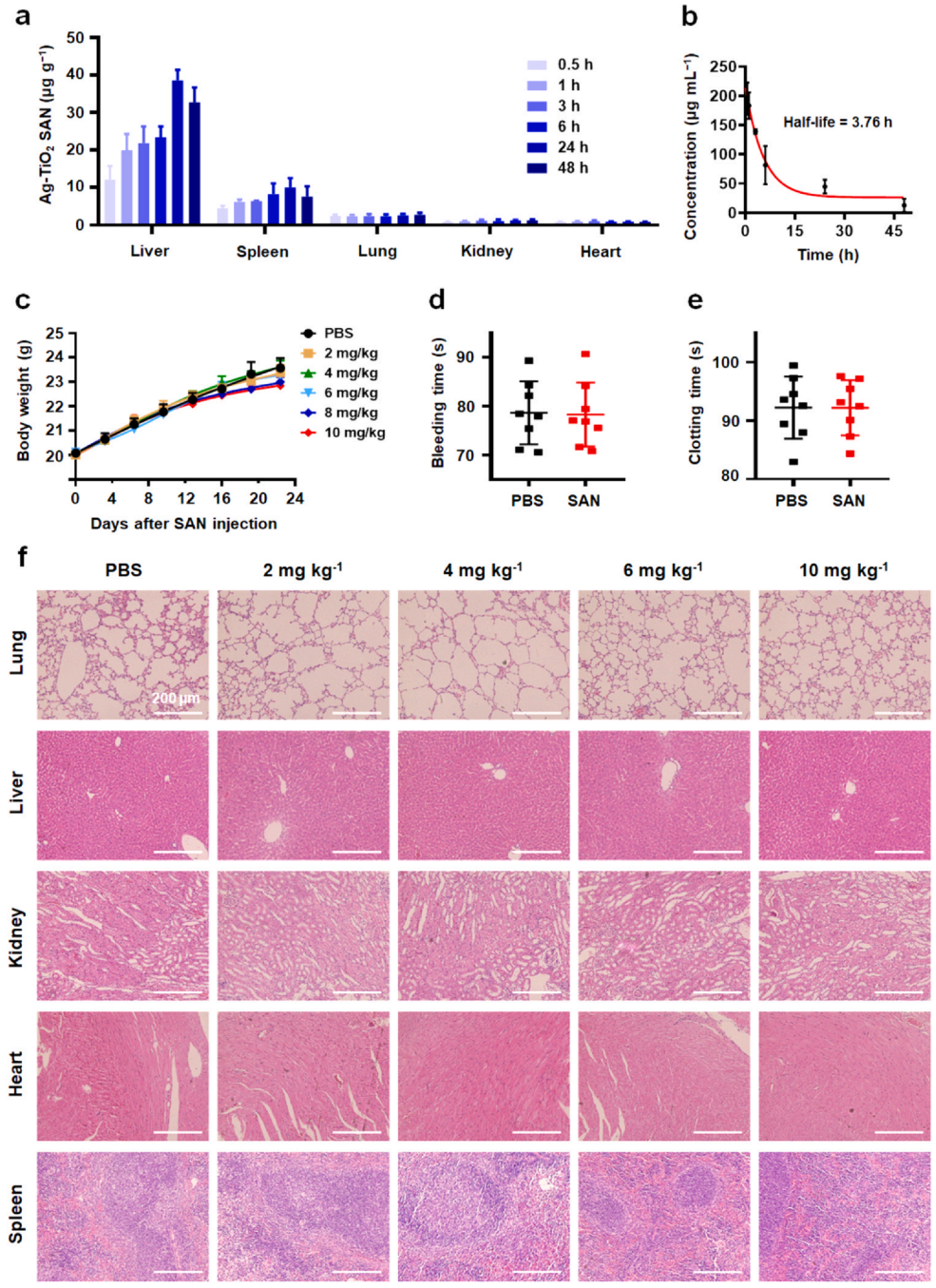

Fig. 5. Pharmacokinetics and biocompatibility of Ag-TiO_2 SAN. (a) The distribution of Ag-TiO_2 SAN, including liver, spleen, lung, kidney, and heart, 0.5–48 h after intravenous administration ($n = 4$). (b) The blood circulation curve of intravenously injected Ag-TiO_2 SAN ($n = 4$). The half-life was calculated to be 3.76 h. (c) Body weight curves of mice that were intravenously injected with PBS or 2–10 mg kg^{-1} Ag-TiO_2 SAN ($n = 10$). (d-e) The statistics of bleeding and clotting times of mice that were intravenously injected with PBS or 10 mg kg^{-1} Ag-TiO_2 SAN ($n = 8$). (f) HE staining of main organs of mice that were intravenously injected with PBS or 2–10 mg kg^{-1} Ag-TiO_2 SAN for 24 days ($n = 3$).

Ag-TiO_2 SAN and S1 RBD, we compared the distribution of superficial amino acids on S1 RBD and serum albumin (67 KD). As shown in Fig. 6b, the percentages of asparagine, glycine, and cysteine are higher on the S1 RBD surface than on the albumin. Subsequently, we investigated the binding conformations of Ag-TiO_2 SAN and the side chains of asparagine, glycine, and cysteine, then calculated their binding energies. In this study, the experimental pH was 7.45 (1% PBS), which is higher than the isoelectric points of asparagine (5.41), glycine (5.97), and cysteine (5.02). Thus the −COOH groups are present in their anion forms and the amino acids are charged with one negative charge. The $Ag@Ti_6O_9(OH)_6$ cluster (Fig. 6c) was used to simulate the NPs with Ag atoms doped on the anatase TiO_2, which was also used in former reports [48]. The binding energies between the side chains of asparagine ($-CH_2C(O)NH_2$), glycine (-H), and cysteine (-SH) with $Ag@Ti_6O_9(OH)_6$ are −11.62, −1.43 and −26.60 kcal mol^{-1}, respectively, indicating that Ag atoms have the strongest

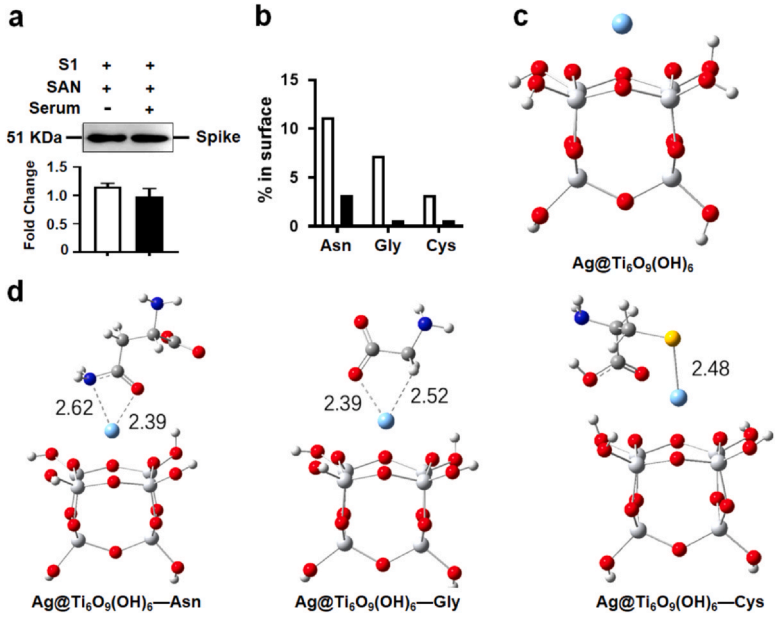

Fig. 6. The theoretical calculation for the interaction of Ag-TiO_2 SAN and S1 RBD. (a) Western blot showing that the interaction of S1 RBD and Ag-TiO_2 SAN is not affected by human serum. (b) Percentages of asparagine (Asn), glycine (Gly), and cysteine (Cys) residues on the surfaces of spike protein and albumin. (c) The geometric structure of the $Ag@Ti_6O_9(OH)_6$ cluster simulating NPs with Ag atoms doped on the anatase TiO_2. (d) The conformations of Asn, Gly and Cys binding with the $Ag@Ti_6O_9(OH)_6$ cluster.

interaction with cysteine because of the strong Ag-S bond. Furthermore, asparagine has medium binding energy because the N-atom of the amide has a lone pair of electrons, which forms a coordination bond with the Ag atoms. Glycine, with the -H side chain, has weak interactions with Ag atoms (Fig. 6d). These data provide solid evidence for the dominant affinity between Ag-TiO_2 SAN and S1 RBD.

SARS-CoV2 infects lung tissues through the respiratory tract, then enters into bloodstream to infect $hACE2^+$ tissues [49]. Thus, we used two models, lung administration and tail injection of the pseudovirus, to evaluate the therapy efficacy of Ag-TiO_2 SAN at different stages of SARS-CoV2 infection. hACE2 transgenic mice were used to evaluate the anti-viral activity of Ag-TiO_2 SAN *in vivo*. The gene expression of hACE2 was confirmed with qPCR analysis (Figure S15a). With Cy5.5 labeled S1 RBD and SARS-CoV2 pseudovirus, we detected high levels of S1 RBD and SARS-CoV2 pseudovirus in the lung tissues of hACE2 transgenic mice from 0 to 24 h. In contrast, the infection of S1 RBD and pseudovirus significantly decreased when lung tissues were pretreated with Ag-TiO_2 SAN. Importantly, the S1 RBD and pseudovirus are almost completely eliminated after 24 h (Fig. 7a–d). In addition, the results of tail injection of the pseudovirus showed that Ag-TiO_2 SAN is effectively anti-SARS-CoV2 *in vivo* (Figure S15b-c), indicating that the SAN is effective antiviral activity both in the early and late stage of SARS-CoV2 infection.

To understand the mechanisms underlying the antiviral effects of Ag-TiO_2 SAN, we tracked the biological location of SAN *in vivo*. As known, macrophages are strategically located throughout the body tissues and liquids, where they non-specifically ingest and process foreign materials [50]. During pathogen infection, macrophages kill or degrade microorganisms by producing ROS and reducing the intracellular pH value [51,52]. Furthermore, many studies have shown that the induction of ROS production by various nanomaterials depends on the acidic environment of lysosomes *in vivo* [53,54]. In order to investigate whether Ag-TiO_2 SAN enhances SARS-CoV2 pseudovirus uptake by macrophages, a viral phagocytosis assay was performed. The mouse macrophage cell line RAW264.7 and the human macrophage cell line THP-1 were induced to M1 phase macrophages. As shown in Figure S16a, the adherent ability of M1 macrophages was increased. In addition, the markers of M1 macrophages were also upregulated compared with M0 macrophages (Figure S16b-c). In the phagocytosis assays, the concentration of SARS-CoV2 pseudovirus in the culture supernatant of mouse and human macrophages was significantly decreased in Ag-TiO_2 SAN treated group than PBS control (Fig. 7e-f), indicating that Ag-TiO_2 SAN promotes SARS-CoV2 pseudovirus uptake of macrophages and subsequent degradation. Finally, in order to understand the mechanisms underlying the anti-SARS-CoV2 effects of Ag-TiO_2 SAN *in vivo*, we tracked the intracellular localization of Ag-TiO_2 SAN by transmission electron microscope (TEM). Fig. 7g-h shows that Ag-TiO_2 SAN colocalized with lysosomes of mouse and human macrophages. More importantly, flow cytometry analysis showed that Ag-TiO_2 SAN significantly increased ROS generation in macrophages (Fig. 7i-j), and this result was confirmed by immunofluorescence assay (Figure S17). Thus, Ag-TiO_2 SAN initially promotes virus uptake by macrophages. Under acid condition of lysosomes of macrophages, the SAN subsequently induces high level of ROS to degrade virus.

According to our results and other studies [51,55], macrophages possess a higher tolerance to ROS than other cells. In this antiviral system, Ag-TiO_2 SAN efficiently eliminated SARS-CoV2 pseudovirus in lysosomes of macrophages. However, this effect did not affect the viability of macrophages. The pseudovirus was degraded by the SAN depending on its intrinsic peroxidase-like activity in lysosomes of macrophages. However, the concentration of Ag-TiO_2 SAN converts

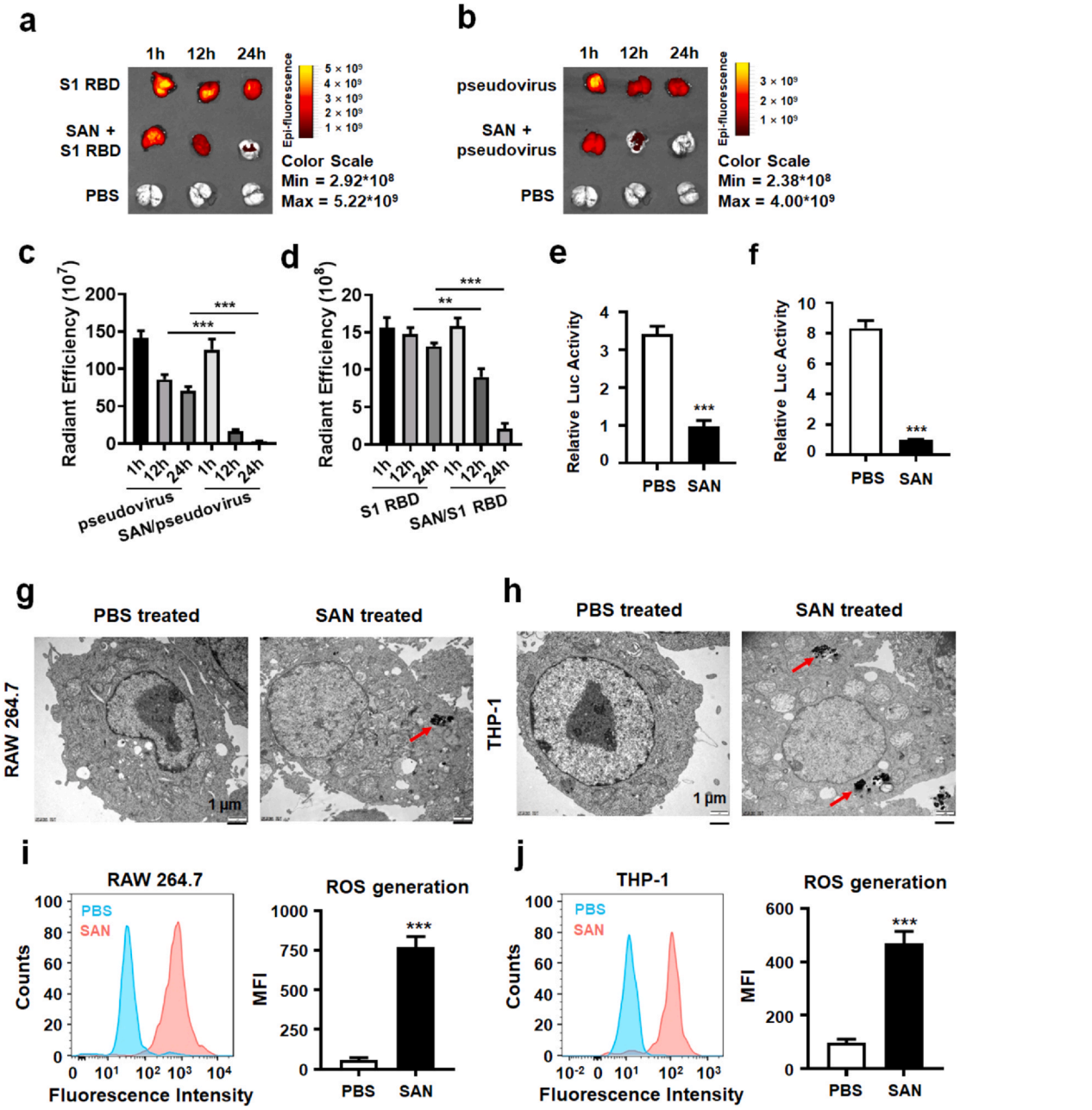

Fig. 7. Antiviral evaluation of Ag-TiO_2 SAN in vivo. (a-b) Small animal imaging for the lung tissues of hACE2 transgenic mice, which were atomized with or without Ag-TiO_2 SAN (10 mg kg^{-1}) for 1 h, then were atomized with Cy5.5 labeled S1 RBD (2 mg per mouse) or SARS-CoV2 pseudovirus ($10^{4.5}$ $TCID_{50}$). The same control (PBS treated) was used in a and b. (c-d) The statistics of radiant efficiency of S1 RBD (c), and pseudovirus (d) infected lung tissues of hACE2 transgenic mice ($n = 3$). (e) Ag-TiO_2 SAN enhances SARS-CoV2 pseudovirus uptake of mouse macrophages. (f) Ag-TiO_2 SAN enhances SARS-CoV2 pseudovirus uptake of human macrophages. (g-h) TEM images show Ag-TiO_2 SAN colocalized with lysosomes of mouse and human macrophages. (i-j) Ag-TiO_2 SAN enhances ROS generation of macrophages.

free radicals is not enough to kill host cells. Cellular viability is also not affected by other nanomaterials with peroxidase-like activity at appropriate concentrations [56,57].

Conclusion

In this study, we designed a TiO_2 supported single atom nanozyme containing 1 wt% atomically dispersed silver atoms (Ag-TiO_2 SAN), which could serve as a highly efficient anti-SARS-CoV2 nanomaterial. First, Ag-TiO_2 SAN displays a high adsorption ability for S1 protein of SARS-CoV2. The pull-down assay suggested that Ag-TiO_2 SAN significantly inhibits the interaction between S1 RBD and its receptor hACE2. By theoretical calculation, we found the interaction between Ag atoms and asparagine and cysteine of S1 RBD. This combination of Ag atoms and amino acids explains the mechanism of high adsorption of SARS-CoV2 pseudovirus by the SAN and inhibition of S1 RBD binding to hACE2. Meanwhile, this nanomaterial exhibits limited toxicity due to its TiO_2 carrier and low Ag atom load, suggesting Ag-TiO_2 SAN can be applied *in vivo* as a nanozyme-based biosafety material. Second, we found that Ag-TiO_2 SAN possesses peroxidase-like activity, producing high level of ROS under acid condition. Third, Ag-TiO_2 SAN enhanced phagocytosis of SARS-CoV2 pseudovirus in macrophages and colocalized with lysosomes, including the production of high levels of ROS due to its peroxidase-like activity. As a result, SARS-CoV2 pseudovirus is broken down. Finally, with viral elimination models, Ag-TiO_2 SAN

efficiently eliminated SARS-CoV2 pseudovirus and spike protein. In summary, we successfully designed and achieved a gram-scale synthesis of a novel SAN for resisting and clearing SARS-CoV2 *via* its high adsorption and peroxidase-like activity.

Statistical Analysis

Results are expressed as the mean ± SD of at least three independent experiments unless otherwise stated. Data were analyzed with GraphPad Prism 8 software (San Diego, CA). The unpaired two-sided student *t*-test was employed to determine the differences between two groups. $^{*}P < 0.05$, $^{**}P < 0.01$, $^{***}P < 0.001$.

CRediT authorship contribution statement

Daji Wang, Bin Zhang, Hui Ding: Designed and performed the experiments, Analyzed the data and wrote the original draft. **Dan Liu, Jianquan Xiang, Zhongjun Li, Hongxia Duan, Jiyan Zheng, Zheng Liu, Bing Jiang, Yang Liu, Ni Xie, Han Zhang:** Analyzed the data and provided valuable advice. **Xuejiao J. Gao:** Methodology, Formal analysis, Wrote original draft. **Xuehui Chen:** Protein structure analysis. **Xiyun Yan, Kelong Fan, Guohui Nie:** Conceptualization, Supervision.

Declaration of Competing Interest

The authors declare that they have no known competing financial interests or personal relationships that could have appeared to influence the work reported in this paper.

Acknowledgments

This work was supported by National Natural Science Foundation of China (81970875, 31530026, 31871005, 31900981, 82003303), Strategic Priority Research Program of CAS (XDB29040101), Key Research Program of Frontier Sciences, CAS (QYZDY-SSW-SMC013), Natural Science Foundation of Guangdong Province (2019A1515011495, 2018A030310665, 2020A151501787), Shenzhen Science and Technology Innovation Committee (JCYJ20170413162242627, ZDSYS201707281114196, JCYJ20190806163814395, JCYJ20180508152528735, JSGG20191129144225464, JCYJ20190806163805286, JCYJ20190809095811254, JCYJ20200109140412476), Sanming Project of Medicine in Shenzhen (SZSM201612031), Beijing Natural Science Foundation of China (7192123), Youth Innovation Promotion Association of Chinese Academy of Sciences (2018122, 2019093), China Postdoctoral Science Foundation Funded Project (2021M692217, 2019M660212), CAS Interdisciplinary Innovation Team (JCTD-2020-08). We thank Dr. Ruofei Zhang (Institute of Biophysics, Chinese Academy of Sciences) for his technical support. We thank Dr. Jiuyang He (Institute of Biophysics, Chinese Academy of Sciences) for language editing.

Appendix A. Supporting information

Supplementary data associated with this article can be found in the online version at doi:10.1016/j.nantod.2021.101243.

References

[1] C. Huang, Y. Wang, X. Li, L. Ren, J. Zhao, Y. Hu, L. Zhang, G. Fan, J. Xu, X. Gu, Z. Cheng, T. Yu, J. Xia, Y. Wei, W. Wu, X. Xie, W. Yin, H. Li, M. Liu, Y. Xiao, H. Gao, L. Guo, J. Xie, G. Wang, R. Jiang, Z. Gao, Q. Jin, J. Wang, B. Cao, Clinical features of patients infected with 2019 novel coronavirus in Wuhan, China, Lancet 395 (2020) 497–506.
[2] C. Wang, P.W. Horby, F.G. Hayden, G.F. Gao, A novel coronavirus outbreak of global health concern, Lancet 395 (2020) 470–473.
[3] R. Lu, X. Zhao, J. Li, P. Niu, B. Yang, H. Wu, W. Wang, H. Song, B. Huang, N. Zhu, Y. Bi, X. Ma, F. Zhan, L. Wang, T. Hu, H. Zhou, Z. Hu, W. Zhou, L. Zhao, J. Chen, Y. Meng, J. Wang, Y. Lin, J. Yuan, Z. Xie, J. Ma, W.J. Liu, D. Wang, W. Xu, E.C. Holmes, G.F. Gao, G. Wu, W. Chen, W. Shi, W. Tan, Genomic characterisation and epidemiology of 2019 novel coronavirus: implications for virus origins and receptor binding, Lancet 395 (2020) 565–574.
[4] L.-F. Wang, D.E. Anderson, Viruses in bats and potential spillover to animals and humans, Curr. Opin. Virol. 34 (2019) 79–89.
[5] T.G. Ksiazek, D.D. Erdman, C.S. Goldsmith, Zaki, T.C.T. Peret, S.L. Emery, S. Tong, C. Urbani, J.A. Comer, W. Lim, A novel coronavirus associated with severe acute respiratory syndrome, N. Engl. J. Med. 348 (2003) 1953–1966.
[6] E. Mahase, Coronavirus covid-19 has killed more people than SARS and MERS combined, despite lower case fatality rate, BMJ 368 (2020) 641.
[7] N. Beyth, Y. Houri-Haddad, A. Domb, W. Khan, R. Hazan, Alternative antimicrobial approach: nano-antimicrobial materials, Evid. -Based Complement. Altern. Med.: eCAM 2015 (2015) 246012.
[8] L. Li, J. Sun, X. Li, Y. Zhang, Z. Wang, C. Wang, J. Dai, Q. Wang, Controllable synthesis of monodispersed silver nanoparticles as standards for quantitative assessment of their cytotoxicity, Biomaterials 33 (2012) 1714–1721.
[9] Y. Yu, F. Bu, H. Zhou, Y. Wang, J. Cui, X. Wang, G. Nie, H.H. Xiao, Effect of titanium on microstructure, texture, and mechanical property of As-extruded Mg—Sn alloy, Front. Mater. 7 (2020) 2428–2434.
[10] X. Zhu, A.F. Radovic-Moreno, J. Wu, R. Langer, J. Shi, Nanomedicine in the management of microbial infection - overview and perspectives, Nano Today 9 (2014) 478–498.
[11] S.R. Bonam, N.G. Kotla, R.A. Bohara, Y. Rochev, T.J. Webster, J. Bayry, Potential immuno-nanomedicine strategies to fight COVID-19 like pulmonary infections, Nano Today 36 (2021) 101051.
[12] K.M. Tripathi, H.T. Ahn, M. Chung, X.A. Le, D. Saini, A. Bhati, S.K. Sonkar, M.I. Kim, T. Kim, N, S, and P-co-doped carbon quantum dots: intrinsic peroxidase activity in a wide pH range and its antibacterial applications, ACS Biomater. Sci. Eng. 6 (2020) 5527–5537.
[13] M. Qin, Z. Cao, J. Wen, Q. Yu, C. Liu, F. Wang, J. Zhang, F. Yang, Y. Li, G. Fishbein, S. Yan, B. Xu, Y. Hou, Z. Ning, K. Nie, N. Jiang, Z. Liu, J. Wu, Y. Yu, H. Li, H. Zheng, J. Li, W. Jin, S. Pang, S. Wang, J. Chen, Z. Gan, Z. He, Y. Lu, An antioxidant enzyme therapeutic for COVID-19, Adv. Mater. 32 (2020) 2004901.
[14] D. Jiang, D. Ni, Z.T. Rosenkrans, P. Huang, X. Yan, W. Cai, Nanozyme: new horizons for responsive biomedical applications, Chem. Soc. Rev. 48 (2019) 3683–3704.
[15] L.H. Dubois, B.R. Zegarski, R.G. Nuzzo, Fundamental studies of microscopic wetting on organic surfaces. 2. Interaction of secondary adsorbates with chemically textured organic monolayers, J. Am. Chem. Soc. 112 (1990) 570–579.
[16] E.E. Oren, C. Tamerler, D. Sahin, M. Hnilova, U.O.S. Seker, M. Sarikaya, R. Samudrala, A novel knowledge-based approach to design inorganic-binding peptides, Bioinformatics 23 (2007) 2816–2822.
[17] J.L. Elechiguerra, J.L. Burt, J.R. Morones, A. Camacho-Bragado, X. Gao, H.H. Lara, M.J. Yacaman, J. Nanobiotechnol. 3 (2005) 6.
[18] L. Gao, J. Zhuang, L. Nie, J. Zhang, Y. Zhang, N. Gu, T. Wang, J. Feng, D. Yang, S. Perrett, X. Yan, Intrinsic peroxidase-like activity of ferromagnetic nanoparticles, Nat. Nanotechnol. 2 (2007) 577–583.
[19] L. Han, C. Li, T. Zhang, Q. Lang, A. Liu, Au@Ag heterogeneous nanorods as nanozyme interfaces with peroxidase-like activity and their application for one-pot analysis of glucose at nearly neutral pH, ACS Appl. Mater. Interfaces 7 (2015) 14463–14470.
[20] F. Gao, G. He, H. Yin, J. Chen, Y. Liu, C. Lan, S. Zhang, B. Yang, Titania-coated 2D gold nanoplates as nanoagents for synergistic photothermal/sonodynamic therapy in the second near-infrared window, Nanoscale 11 (2019) 2374–2384.
[21] Q. Liang, J. Xi, X.J. Gao, R. Zhang, Y. Yang, X. Gao, X. Yan, L. Gao, K. Fan, A metal-free nanozyme-activated prodrug strategy for targeted tumor catalytic therapy, Nano Today 35 (2020) 100935.
[22] A. Panáček, L. Kvítek, M. Smékalová, R. Večeřová, M. Kolář, M. Röderová, F. Dyčka, M. Šebela, R. Prucek, O. Tomanec, R. Zbořil, Bacterial resistance to silver nanoparticles and how to overcome it, Nat. Nanotechnol. 13 (2018) 65–71.
[23] P. Dibrov, J. Dzioba, K.K. Gosink, C.C. Häse, Chemiosmotic mechanism of antimicrobial activity of Ag(+) in Vibrio cholerae, Antimicrob. Agents Chemother. 46 (2002) 2668–2670.
[24] Y. Li, Z. Lin, M. Zhao, T. Xu, C. Wang, L. Hua, H. Wang, H. Xia, B. Zhu, Silver nanoparticle based codelivery of oseltamivir to inhibit the activity of the H1N1 influenza virus through ROS-mediated signaling pathways, ACS Appl. Mater. Interfaces 8 (2016) 24385–24393.
[25] K. Zheng, M.I. Setyawati, T.P. Lim, D.T. Leong, J. Xie, Antimicrobial cluster bombs: silver nanoclusters packed with daptomycin, ACS Nano 10 (2016) 7934–7942.
[26] S.U. Khan, M. Al-Shahry, W.B. Ingler Jr., Efficient photochemical water splitting by a chemically modified n-TiO2, Science 297 (2002) 2243–2245.
[27] T. Rasheed, M. Adeel, F. Nabeel, M. Bilal, H.M.N. Iqbal, TiO2/SiO2 decorated carbon nanostructured materials as a multifunctional platform for emerging pollutants removal, Sci. Total Environ. 688 (2019) 299–311.
[28] S.Y. Choi, B. Cho, Extermination of influenza virus H1N1 by a new visible-light-induced photocatalyst under fluorescent light, Virus Res 248 (2018) 71–73.
[29] S. Ma, S. Zhan, Y. Jia, Q. Zhou, Superior antibacterial activity of Fe3O4-TiO2 nanosheets under solar light, ACS Appl. Mater. Interfaces 7 (2015) 21875–21883.
[30] J. Meng, P. Zhang, F. Zhang, H. Liu, J. Fan, X. Liu, G. Yang, L. Jiang, S. Wang, A self-cleaning TiO2 nanosisal-like coating toward disposing nanobiochips of cancer detection, ACS Nano 9 (2015) 9284–9291.
[31] L. Huang, J. Chen, L. Gan, J. Wang, S. Dong, Single-molecule detection of biomarker and localized cellular photothermal therapy using an optical microfiber with nanointerface, Sci. Adv. 5 (2019) eaax4659.
[32] S. Zhao, G. Chen, G. Zhou, L.C. Yin, J.P. Veder, B. Johannessen, M. Saunders, S.Z. Yang, R. De Marco, C. Liu, A universal seeding strategy to synthesize single

atom catalysts on 2D materials for electrocatalytic applications, Adv. Funct. Mater. 30 (2020) 1906157.
[33] M.S. Kim, J. Lee, H.S. Kim, A. Cho, K.H. Shim, T.N. Le, S.S.A. An, J.W. Han, M.I. Kim, J. Lee, Heme cofactor-resembling Fe–N single site embedded graphene as nanozymes to selectively detect H2O2 with high sensitivity, Adv. Funct. Mater. 30 (2020) 1905410.
[34] W. Zhang, W. Zheng, Single atom excels as the smallest functional material, Adv. Funct. Mater. 26 (2016) 2988–2993.
[35] B. Zhang, H. Asakura, J. Zhang, J. Zhang, S. De, N. Yan, Stabilizing a platinum1single-atom catalyst on supported phosphomolybdic acid without compromising hydrogenation activity, Angew. Chem. 128 (2016) 8459–8463.
[36] B. Zhang, T. Fan, N. Xie, G. Nie, H. Zhang, Versatile applications of metal single-atom @ 2D material nanoplatforms, Adv. Sci. (Weinh., Baden. -Wurtt., Ger.) 6 (2019) 1901787.
[37] H. Xiang, W. Feng, Y. Chen, Single-atom catalysts in catalytic biomedicine, Adv. Mater. 32 (2020) 1905994.
[38] B. Xu, H. Wang, W. Wang, L. Gao, S. Li, X. Pan, H. Wang, H. Yang, X. Meng, Q. Wu, L. Zheng, S. Chen, X. Shi, K. Fan, X. Yan, H. Liu, A single-atom nanozyme for wound disinfection applications, Angew. Chem. Int Ed. Engl. 58 (2019) 4911–4916.
[39] L. Huang, J. Chen, L. Gan, J. Wang, S. Dong, Single-atom nanozymes, Sci. Adv. 5 (2019) 5490.
[40] S. Xia, M. Liu, C. Wang, W. Xu, Q. Lan, S. Feng, F. Qi, L. Bao, L. Du, S. Liu, C. Qin, F. Sun, Z. Shi, Y. Zhu, S. Jiang, L. Lu, Inhibition of SARS-CoV-2 (previously 2019-nCoV) infection by a highly potent pan-coronavirus fusion inhibitor targeting its spike protein that harbors a high capacity to mediate membrane fusion, Cell Res. 30 (2020) 343–355.
[41] M. Hoffmann, H. Kleine-Weber, S. Schroeder, N. Kruger, T. Herrler, S. Erichsen, T.S. Schiergens, G. Herrler, N.H. Wu, A. Nitsche, M.A. Muller, C. Drosten, S. Pohlmann, SARS-CoV-2 cell entry depends on ACE2 and TMPRSS2 and is blocked by a clinically proven protease inhibitor, Cell 181 (2020) 271–280 e278.
[42] S. Liao, Y. Zhang, X. Pan, F. Zhu, C. Jiang, Q. Liu, Z. Cheng, G. Dai, G. Wu, L. Wang, L. Chen, Antibacterial activity and mechanism of silver nanoparticles against multidrug-resistant Pseudomonas aeruginosa, Int J. Nanomed. 14 (2019) 1469–1487.
[43] S.J. Soenen, P. Rivera-Gil, J.M. Montenegro, W.J. Parak, S.C.D. Smedt, K. Braeckmans, Cellular toxicity of inorganic nanoparticles: Common aspects and guidelines for improved nanotoxicity evaluation, Nano Today 6 (2011) 446–465.
[44] A.E. Nel, L. Mädler, D. Velegol, T. Xia, E.M. Hoek, P. Somasundaran, F. Klaessig, V. Castranova, M. Thompson, Understanding biophysicochemical interactions at the nano-bio interface, Nat. Mater. 8 (2009) 543–557.
[45] K.S. Siddiqi, A. Husen, R.A.K. Rao, A review on biosynthesis of silver nanoparticles and their biocidal properties, J. Nanobiotechnol. 16 (2018) 14.
[46] J.L. Elechiguerra, J.L. Burt, J.R. Morones, A. Camacho-Bragado, X. Gao, H.H. Lara, M.J. Yacaman, Interaction of silver nanoparticles with HIV-1, J. Nanobiotechnol. 3 (2005) 6.
[47] Y.C. Chung, I.H. Chen, C.J. Chen, The surface modification of silver nanoparticles by phosphoryl disulfides for improved biocompatibility and intracellular uptake, Biomaterials 29 (2008) 1807–1816.
[48] A.S. Hussain, M.L. McKee, J.M. Heinzel, X. Sun, B.J. Tatarchuk, Density functional theory study of organosulfur selective adsorption on Ag–TiO2 adsorbents, J. Phys. Chem. C 118 (2014) 14938–14947.
[49] M. Wadman, J. Couzin-Frankel, J. Kaiser, C. Matacic.
[50] P.J. Murray, T.A. Wynn, Protective and pathogenic functions of macrophage subsets, Nat. Rev. Immunol. 11 (2011) 723–737.
[51] T.A. Wynn, A. Chawla, J.W. Pollard, Macrophage biology in development, homeostasis and disease, Nature 496 (2013) 445–455.
[52] Y. Lavin, A. Mortha, A. Rahman, M. Merad, Regulation of macrophage development and function in peripheral tissues, Nat. Rev. Immunol. 15 (2015) 731–744.
[53] L. Liu, Y. Wei, S. Zhai, Q. Chen, D. Xing, Dihydroartemisinin and transferrin dual-dressed nano-graphene oxide for a pH-triggered chemotherapy, Biomaterials 62 (2015) 35–46.
[54] C. Yin, H. Zhu, C. Xie, L. Zhang, P. Chen, Q. Fan, W. Huang, K. Pu, Organic nanoprobe cocktails for multilocal and multicolor fluorescence imaging of reactive oxygen species, Adv. Funct. Mater. 27 (2017) 1700493.
[55] B. Patella, M. Buscetta, S. Di Vincenzo, M. Ferraro, G. Aiello, C. Sunseri, E. Pace, R. Inguanta, C. Cipollina, Electrochemical sensor based on rGO/Au nanoparticles for monitoring H2O2 released by human macrophages, Sens. Actuators B: Chem. 327 (2021) 128901.
[56] G. Yim, C.Y. Kim, S. Kang, D.-H. Min, K. Kang, H. Jang, Intrinsic peroxidase-mimicking Ir nanoplates for nanozymatic anticancer and antibacterial treatment, ACS Appl. Mater. Interfaces 12 (2020) 41062–41070.
[57] W.C. Hu, M.R. Younis, Y. Zhou, C. Wang, X.H. Xia, In situ fabrication of ultrasmall gold nanoparticles/2D MOFs hybrid as nanozyme for antibacterial therapy, Small 16 (2020) 2000553.